Predicting the yield stress of a 3D printed porous material from its internal structure

Martin Lesueur[1,*+], Thomas Poulet[2,+], and Manolis Veveakis[1,+]

[1]Duke University, Civil and Environmental Engineering, Durham, 27708, USA
[2]CSIRO, Mineral Resources, Perth, 6151, Australia
[*]martin.lesueur@duke.edu
[+]these authors contributed equally to this work

ABSTRACT

The design of any engineering structure requires the knowledge, and therefore determination, of the yield, i.e. limit of elasticity, for the building material. Whilst destructive experimental testing is currently necessary to do so, our work is part of initiatives which aim at deriving the yield without such laboratory experiments. The seminal work of Gurson (1977) on a simplified pore structure, a single spherical pore, first provided a theoretical relationship between the yield stress and the porosity. Specifically, it showed that the presence of pore space is responsible for the existence of a compression cap in plasticity, in addition to lowering the yield stress. This contribution extends the approach to determine the macroscopic yield of a porous material by taking explicitly into account its internal structure. As the yielding of a porous material is controlled by the geometry of its internal structure, we postulate that it is nearly independent of the constitutive plastic behaviour of the material. Here, we show that the influence of that internal structure on the yield could be retrieved from a finite element computation with just an elasto-plastic ideal material equivalent of the skeleton's. With some basic knowledge about the skeleton's mechanical properties, this process allows the determination of the yield stress without requiring the experimental compression of the material. We showcase the predictive power of the method against experimental testing, initially for a unique spherical void in a 3D-printed cylinder sample following Gurson, before demonstrating its applicability on a complex 3D-printed rock microstructure, reconstructed from segmented micro-Computerised Tomography scans.

Introduction

Many studies are aiming at accounting for the influence of the material's internal structure on a its mechanical properties, whether on elastic modulus[1,2], strength[3–6], or plastic flow law[5,6], to cite only a few. This contribution focuses on the yield value, which is important for two reasons. By definition, it points to the limit of elasticity, which is necessary for the design of structures to prevent them from entering plastic regime and suffer irreversible deformations. On top of this, when the plastic regime is expected, knowledge of the yield surface is necessary to model a material's plastic behaviour[7].

The only unambiguous determination of mechanical yield point, as a limit of elasticity, is possibly restricted to the simplest case of ideal non-porous linear elastic and ideally plastic materials, like metals for instance. Indeed, experimental compression tests of such materials lead to characteristic stress-strain curves displaying a sharp transition between the linear elasticity and plasticity, where strain increases at constant stress. For more complex materials, however, including real geomaterials like porous rocks, the notion of macroscopic yield stress is more ambiguous and its determination dependent on the method selected. To alleviate this ambiguity we use the following three definitions of yield from the sixth edition of the McGraw-Hill Dictionary of Scientific and Technical Terms[8]:

- ***yield*** *[MECHANICS] That stress in a material at which plastic deformation occurs.*
- ***yield point*** *[MECHANICS] The lowest stress at which strain increases without increase in stress.*
- ***yield strength*** *[MECHANICS] The stress at which a material exhibits a specified deviation from proportionality of stress and strain.*

The first definition, referred to as **initial yield** in this contribution corresponds to the stress when the first region in the material undergoes plasticity. This value is not particularly useful since not easily measurable[9]. The second definition, commonly named **limit load**, points to the state of collapse of the material. The last definition is the **macroscopic yield**, which is the focus in this contribution because it really points to the limit of linear elasticity at the scale of the sample, necessary for structure design. Additionally, it is a necessary parameter for any modelling of plasticity. This yield is classically measured experimentally on stress-strain curves using the classical offset method[10], as the intersection of the curve with a line parallel to

the initial linear-elastic part of that curve, shifted by an ad-hoc strain threshold. In this contribution, following Lesueur *et al.*[11], the macroscopic yield is measured on stress-strain curves with an energetic method, which provides similar values but with stronger physical meaning. It is necessary to try and reduce the use of destructive methods for its measurement, particularly when material samples are difficult to obtain in sufficient quantity, which is the case in subsurface operations like petroleum engineering for instance. Two alternatives are possible.

The first one is to find relationships to link the yield to properties that can be measured with non-destructive tests. Some models already account for the impact on yield from the simplest parameter characterising the internal structure: porosity[5,6,12]. Through these models, we know that the presence of pore space is responsible for the existence of a compression cap of plasticity, in addition to lowering the yield stress value. We focus specifically in this contribution on Gurson[5], who developed a criterion to predict the limit load of a material from its porosity. He considered the simplest configuration, which consists of a single spherical pore. To avoid any non-essential complexity and restrict the study to the influence of porosity, he selected a rigid and ideally plastic material, which ensured that the relationships extracted were indeed be attributed solely to the porosity without any interfering influence of any other material properties. The outer geometry of the unit cell was taken as spherical, like the void shape, in order to retain the geometrical isotropy benefits from the symmetry in the analysis. Using the upper-bound limit analysis method, Gurson obtained an approximate upper solution to the limit load of the hollow sphere geometry, which proved to be precise enough to fit experimental data[13,14]. Extending his work, numerous studies followed which improved on the model, including derivations accounting for other shapes of voids (e.g. elliptical[15]), the interaction between voids[16,17], or the consideration of more complex matrix materials (e.g. viscoplasticity[18]). That type of analysis was an important first step in our understanding of the influence of the internal structure. Yet, because of its use of limit analysis, its applicability is restricted to the limit load value and corresponding results have not yet been derived for the more practical definition of yield, the macroscopic yield. In addition, porosity, as a scalar field, only represents one of the characteristics[19] and can therefore not capture all geometrical effects, with more work remaining from a more general perspective. Specifically in this contribution, we define the internal structure as the structure of the porous material's skeleton. In the case of 3D printed porous scaffolds, it is directly the internal geometry of the unit cell. In the case of natural materials bones or rocks, it is delimited in segmented micro-Computerised Tomography (μCT) scans by the pore space boundary.

The second alternative is to numerically obtain the stress-strain curve. With recent computational advances, it is now possible to simulate mechanical deformation of a Representative Element Volume (REV) of the material (e.g.[20]). At that size, the mechanical behaviour of the volume considered should be representative of the whole sample at the larger scale. Therefore stress-strain curves of the REV can be produced numerically and be comparable to the experimental ones. However, reproducing numerical stress-strain curves of real materials remains difficult. Such simulations require indeed a high mesh resolution to match the REV with accurate grain shapes. The computational cost is amplified by the fact that non-trivial constitutive plastic law are usually implemented to reproduce the behaviour of the material. Indeed, characterising the plastic behaviour of a real material is no easy feat as there exist numerous constitutive models[21], some of which that require many parameters to be calibrated[7].

We take inspiration from both approaches for the solution we suggest in this contribution. We propose to extend Gurson's type of analysis from limit load to macroscopic yield and from porosity to the explicit geometry of the internal structure. To do so, we simulate mechanical compressions on the digitised internal structure and determine the yield with the energetic method from the stress-strain curves computed. By narrowing our study to the determination of yield, we only need to simulate the initial phase of plasticity. The plastic regime starts at the initial yield since theoretically speaking, the material is, from that point on, undergoing localised plastic deformations. However, for porous materials, it is instinctive that the initial yield does not coincide with the macroscopic yield. Localised heterogeneities in the material will indeed fail before the overall response of the material can visually deviate from linearity[9]. Under ongoing deformation, from the initial yield to the macroscopic yield, an arbitrarily small plastic strain is accumulated (as defined by the offset method). However, we conjecture that plasticity does not noticeably affect the material's response until the macroscopic yield. This hypothesis is tested in this contribution by verifying that the yield of a porous material is equal to the one of a virtual porous material with an equivalent ideal elasto-plastic skeleton, instead of considering its more realistic plastic behaviour (including rheology).

The material selected in this contribution is 3D printed polylactic acid (PLA), whose mechanical response from laboratory experiments is plotted in Fig. 1 and modelled in Methods. 3D printing presents great advantages for the experimental validation of our approach. As observed by the superposition of curves in Fig. 1 or Fig. S4, the printed material has a very reproducible behaviour. In addition, the 3D printing technique allows a perfect control of the internal structure of the samples, whose influence we are characterising. 3D printed PLA is particularly well-suited to test our hypothesis because its plastic response is far from ideal plastic (see Fig. 1). This material displays a strong viscoplasticity and we selected a sample size such that deformation pattern is shearbanding, which results in a weakening before reaching the limit load (see Fig. 1), for added complexity. Moreover, the printing process itself influences the plastic properties of the resulting material, as discussed in Methods and Supplementary text, which adds an extra layer of complexity. It is therefore extremely interesting to select this

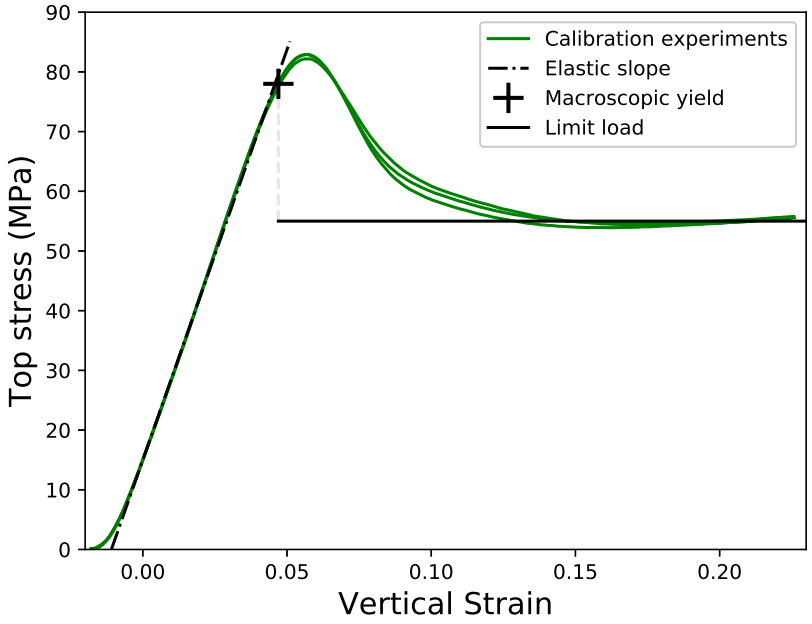

Figure 1. Three stress strain curves of uniaxial compression of 3D printed full cylinders of PLA to observe the plastic response of the material and assess the reproducibility of mechanical tests on 3D printed samples. Our suggested elasto-plastic model is superposed to the curves and determined by three parameters: the slope of the linear elastic part, the macroscopic yield value, and the limit load (displayed on a wide range of strain for visualisation purposes).

material to test our approach, which eliminates the need for characterisation of the viscoplasticity and weakening law of the printed PLA.

To validate the approach proposed, we select at first the simplest internal structure which is the unique spherical pore as Gurson studied. This simple structure allows the 3D printed internal geometry to be very accurate and improve reproducibility of this benchmark. The second part of this contribution presents an application for a more complex internal structure, reconstructed from a rock's segmented µCT scans.

Results

Prediction of the internal structure influence on 3D-printed PLA yield

The objective of this section is to verify if a simplified numerical model can correctly predict the yielding of printed PLA sample with a given internal structure. The printed samples are cylinders containing a spherical void of varying diameter at their centre, specifically of 0.6 and 0.7 (normalised to the cylinder diameter). Due to the Fused Deposition Modeling (FDM) principle of printing, the molten filament is deposited vertically on the sample, which makes it impossible for this technique to print perfectly any overhanging part with an angle greater than 45º. Unfortunately, this is the case of the spherical void with the overhang going to 90º at the top of the sphere. To help the printing, FDM usually relies on printing under these overhangs some support structure that the user can remove after the print is finished. However, our overhang is fully enclosed in the structure so this technique cannot be used without any support structure and we can only assess the quality of the print visually by cutting the sample after the experiments, as shown in Fig. 2. We can see that the quality of the print remained acceptable, even though imperfect. Indeed, during the mechanical compression, this top part of the sphere is the location which experiences the minimum of stress overall.

The samples are subjected to uniaxial compression and the experimental results are plotted in Fig. 3 for the two different sphere diameters. Note that each test is repeated two times for reliability reasons. The good superposition of all curves shows that the results of hollow cylinders experiments are as reproducible as the full ones. The resulting curves for the porous cylinders display sequentially a hardening and a softening phase, before converging to a limit load. Note that an eventual hardening occurs artificially due to the increase of the surface area of contact, which is disregarded. All in all, the mechanical behaviours of the porous samples are very similar to the one for a full sample but with increasingly lower and faster transition to plasticity

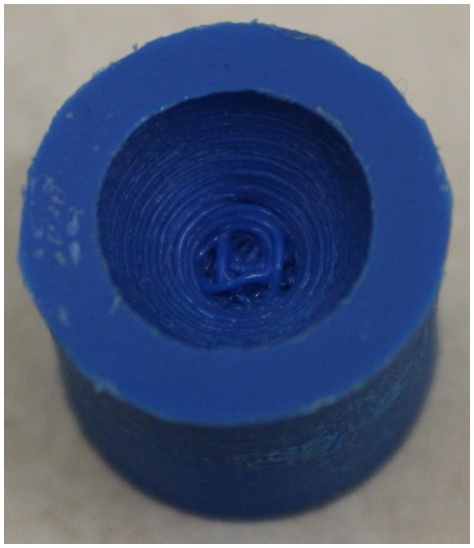

Figure 2. Visualisation of the printing quality of the top of the spherical void of the hollow cylinder. Only the top half of the hollow cylinder was printed for visualisation purposes and the sample is displayed upside down.

as porosity increases.

In this section, we are looking at predicting the influence of the internal structure of the hollow cylinders on two characteristic yield points of the printed PLA: the limit load, studied by Gurson, and as an extension of his study, the macroscopic yield. We used the mechanical simulator of the Finite Element platform MOOSE[22] for all numerical simulations in this contribution. It solves for the momentum balance of the skeleton of the porous material. In our simulation, the skeleton's material is attributed the elastic parameters measured for the printed PLA and for the plasticity, we use a $J2$ rate-independent model with no hardening or softening, defined by our single parameter of interest, the yield point.

The evolutions of the two yields with the internal structure are simulated separately, for each yield. Each simulation is run using the same model with respectively the macroscopic yield and the limit load value of Fig. 1 as the single plastic parameter of the skeleton. The set of simulations is performed twice, for the two geometries of different hole diameters, meshed with second order tetrahedra. The results are displayed in Fig. 3, following the layout introduced in Fig. 1. The stress value of the macroscopic yield of the porous material, measured on the stress-strain curve produced by the first simulation, is reported of Fig. 1 as a cross on the elastic slope measured from the simulation. The stress value of the limit load is retrieved by taking the limit load value of the second simulation and is reported as a solid line in Fig. 1, regardless of the strain value at which it is actually reached.

The comparison of the numerical and experimental results of Fig. 3, quantified in Table. 1, shows that the simulation is matching closely the two properties of plasticity considered, the macroscopic yield and the limit load value, obtained experimentally. Interestingly, this perfect fit, with the numerical limit load matching the stress plateau obtained experimentally as shown in Fig. 3, demonstrates that the influence of the microstructure on a real material's yield can be retrieved even with an idealised model without taking into account the intrinsic behaviour of the real material. This verification validates the hypothesis suggested in the introduction that plasticity has little influence on the porous material's behaviour before the macroscopic yield. Particularly, we showed in this section that the hardening and softening behaviour of the 3D printed PLA does not influence the value of the macroscopic yield in this recognised benchmarking example. This conclusion highlights the potential of the numerical approach to extract the impact of the internal structure on the yield despite an idealised modelling of the material.

Application to rock microstructure

The advantage of studying a single pore compared to any arbitrary internal structure is that this geometry was designed as an idealised REV of rock microstructure. Gurson's theory on the hollow sphere proved to be able to fit real data[13,14]. As a natural extension, we therefore select a rock's microstructure as a more complex geometry in this section for further validation of the suggested approach. The selected rock is a 0.5 mm^3 subsample of the Berea sandstone[23].

Using the stack of segmented 2D μCT scan images, the geometry is meshed in 3D following the methodology described by Lesueur *et al.*[24]. In order to be processed by the Ultimaker 3 machine for printing, the mesh is converted to an STL file format. The sample is printed as a cube of 22 mm^3 size. The quality of the printed sample is quite remarkable in terms of details, capturing very well the overall complexity of the original rock, even though the quality of the print remains imperfect,

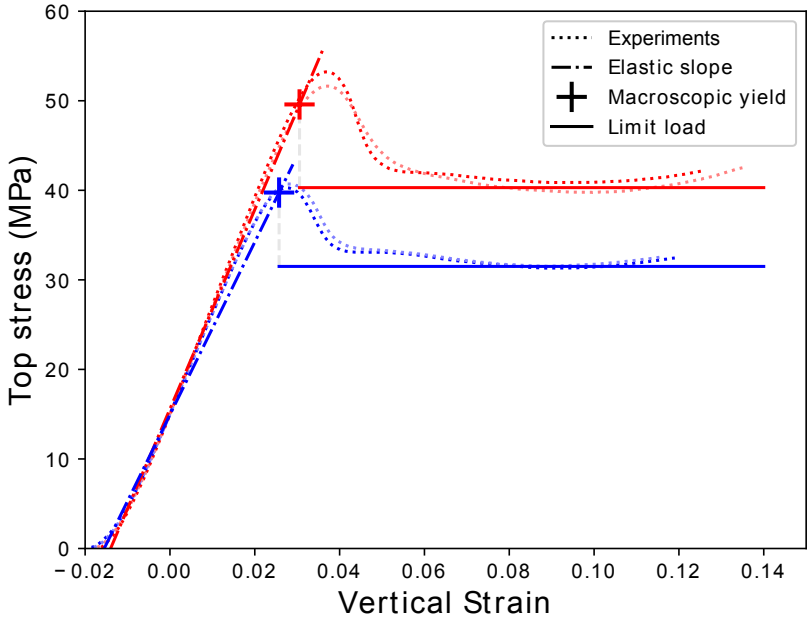

Figure 3. Four stress strain curves of uniaxial compression of 3D printed cylinders of PLA containing a spherical void of different normalised diameters: 0.6 in red and 0.7 in blue. The results of the simulation (elasticity and characteristic plastic points) using the model presented in Methods are superposed to the experimental results.

Table 1. Mechanical properties measured for the experimental and numerical results of the uniaxial compression of hollow cylinders.

Void diameter (normalised)	0.6			0.7		
Specimen number	exp 1	exp 2	**simulation**	exp 1	exp 2	**simulation**
Young's modulus (MPa)	1215	1181	1113	1123	1122	964
Macroscopic yield (MPa)	49.30	47.34	49.59	36.88	37.58	39.75
Limit load (MPa)	40.85	39.78	40.30	31.3	31.51	31.50

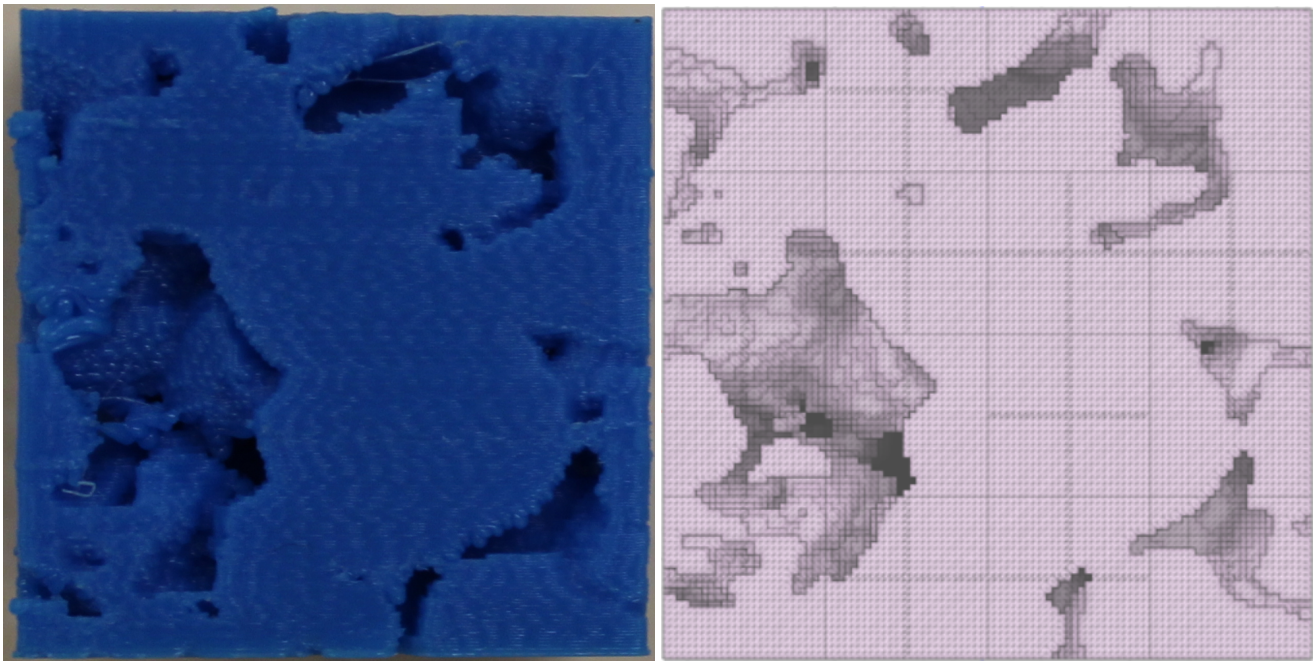

Figure 4. Side face of the printed microstructure (a) compared to the digital rock (b). The whole microstructures can be visualised as 3D figures in Supplementary Material (Fig. S5).

as can be seen in Fig. 4, due to the 45º limit of any overhang discussed in Methods. The printing quality can be assessed by comparing the two 3D figures (see Fig. S5 in Supplementary Material) that visualise the pore space respectively from the original µCT scan and the 3D printed version which was µCT scanned after being printed.

Five identically printed samples are then tested in uniaxial compression following the experimental procedure described in Methods, with a loading speed of 0.08 mm/min. The resulting stress strain curves, plotted in Fig. 5, all have the same general shape, including the same elastic properties and plastic hardening, but noticeably different values of macroscopic yields. We can only infer that the lack of reproducibility is due to the insufficient printing resolution and quality because the curves of Fig. 3, whose samples' printing quality was high, superposed completely. Compared to Fig. 3, the complex internal structure plays a different role than the idealised single pore: the sample shows no softening nor limit load, but instead hardens continuously. The complex pore network in the µCT scan results in a very disperse pore collapse over the whole sample (see plastic deformations in Fig. 6) that could prevent therefore a homogeneous shearband to form, which would explain the absence of softening.

In order to numerically determine the yield of this example, we simulate the same compression on a digital version of that same microstructure, reconstructed from µCT scans and meshed following the method of Lesueur *et al.*[24]. In order to retrieve exclusively the influence of the internal structure on the yield, we take an ideal $J2$ model for the plasticity of the matrix materia. We calibrate this model to resemble the behaviour of the printed PLA, on the response of 3D printed PLA cubes of 22 mm^3 size. Eventually the elasto-plastic model selected is an isotropic linear elasticity with a Young's modulus of 875 MPa and a Poisson ratio of 0.45 and a yield point of 70 MPa, calibrated on the yield measured. The resulting stress strain curve is plotted in Fig. 5.

We note that for both numerical and experimental approach, we do not reach indeed a limit load like in Fig. 3. This confirms our interest in extending Gurson's exclusive study of the limit load to the macroscopic yield because the limit load does not exist for every material.

Despite the fact that the match of Fig. 5 is not as impressive as the one from Fig. 3, the numerical and experimental curves still match qualitatively and display a similar shape. In this more complex example, the porous material appears to be stiffer and stronger (higher macroscopic yield) with the experimental approach. This could be explained by the reinforcement of the structure due to the existence of artificial bridges between pores that were created during the imperfect printing process. The suboptimal printing quality adds to the uncertainty of the experimental results, which brings us more confidence in the value of elasticity and macroscopic yield determined with the numerical approach.

Discussion

In this contribution we presented an approach to determine the macroscopic yield of a porous material from finite element compression of its internal structure, replacing the traditional destructive testing approach. By focusing the study on the

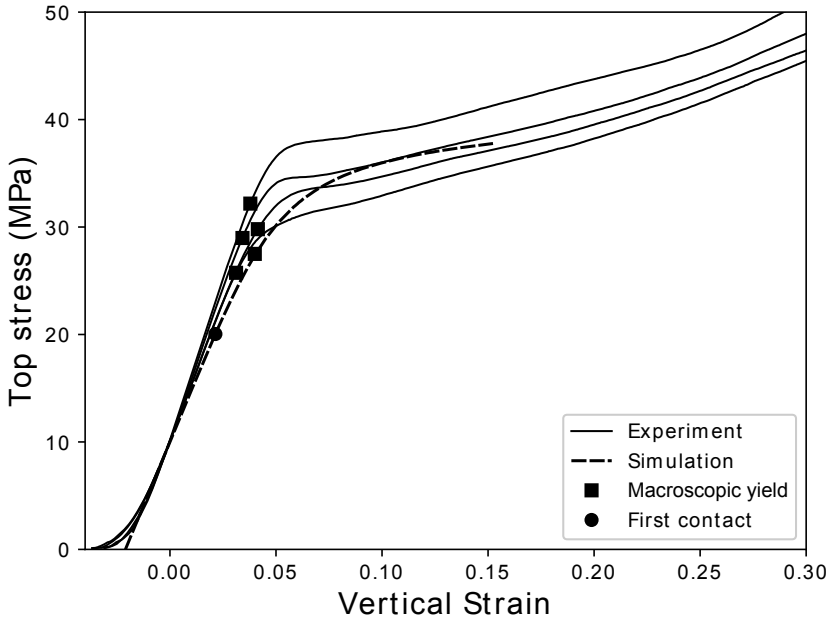

Figure 5. Experimental and numerical stress-strain curves of the uniaxial compression of 3D printed samples of the Berea sandstone[23].

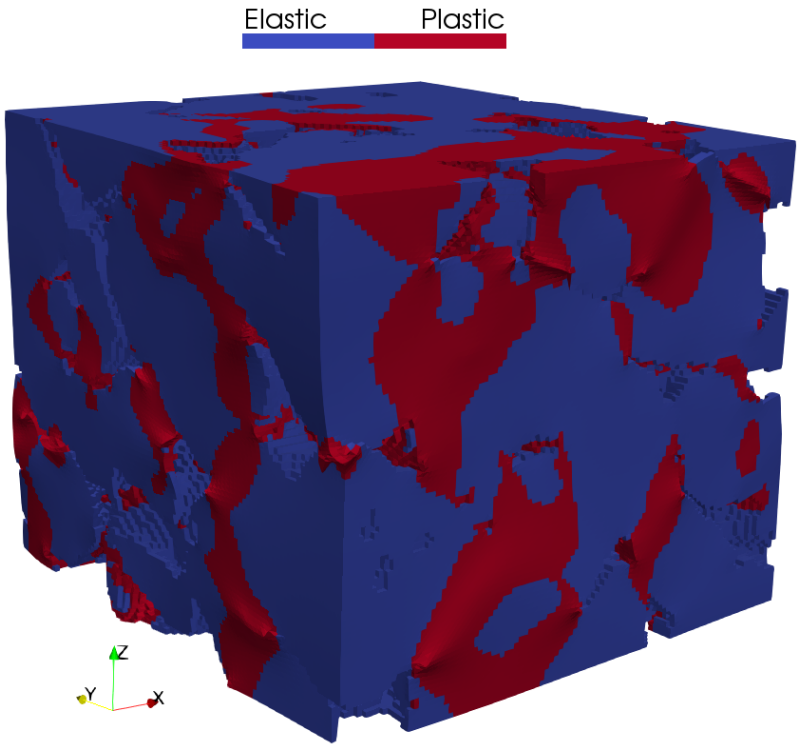

Figure 6. Visualisation of plastic deformations on the numerical uniaxial compression of Fig. 5 at 12% strain.

macroscopic yield instead of the full mechanical behaviour, we have shown that the complex skeleton material can be satisfactorily approximated by an equivalent ideal elasto-plastic material before reaching the macroscopic yield. By reducing the complexity of the material implemented, simulations of mechanical compressions become more accessible.

The new approach was validated on 3D printed PLA. The homogeneity of this material and the reproducibility of the 3D printing techniques makes it a material very suitable for our approach. Furthermore, we show in the Appendix that the plastic behaviour of the material presents a difficult calibration as it depends on many printing parameters. This justifies the use of our approach which disregards this exact plastic behaviour.

To be able to generalise the applicability of the method, we tested the approach against both a simple and complex internal structures. In order to refine the benchmarking of complex internal structure, more suitable 3D printing techniques could be used in order to obtain a quality high enough to obtain perfectly reproducible and therefore trustful results. Indeed, 3D printing μCT scans with high resolution was achieved for instance by Ishutov *et al.*[25].

Since the method was validated against an already challenging material, 3D printed PLA, that displays softening and hardening behaviour, we expect the approach to apply also for a wider range of materials such as geomaterials. To improve the accuracy of our approach in this case, contact mechanics could be implemented as we have shown in Fig. 5 that contacts in a real rock microstructure happen early on the stress-strain curve. It is however unclear if this would affect the macroscopic yield. In any case, contact forces have been known to be responsible for the pressure sensitivity of the yield surface at the macro-scale, modelled commonly with a Drucker-Prager which characterises a wide array of geomaterials.

In summary, this study aimed at highlighting the predictive power scientific community can develop as 3D printing technology is maturing, at a level of quality where reproducible mechanical compression experiments on 3D printed samples can be performed. We showed that the macroscopic yield can be obtained for a given internal structure from 3D printed reproductions, for high enough resolutions. More importantly, it was shown that it can also be predicted numerically, in a non-destructive manner, using the simplest plasticity model for the actual filler material. This result has striking repercussions for a number of applications, including 3D printed scaffolds, or even more for real materials like bones or geomaterials, whose internal structure can be obtained from μCT scans. Given that 3D printing and numerical simulations are approaching their originally anticipated goal of providing invaluable insight to the mechanical properties of natural materials, studies like the present one are aiming at opening the door to an enhanced material design era.

Methods

3D printing and mechanical testing procedure

In recent years, many 3D printing methods have been made available, see review from Dizon *et al.*[26]. Without loss of generality we choose to work with the standard Fused Deposition Modeling (FDM) on the Ultimaker 3 machines of the Innovation co-Lab of Duke University, with a nozzle of 0.4mm diameter. The machine offers the possibility to print multiple materials (see exhaustive list[1] from the manufacturer), with polylactic acid (PLA) and acrylonitrile butadiene styrene (ABS) two of the most commonly used in mechanical testing of 3D printed materials[26,27]. Without any preferences, we choose to work with PLA.

Many of the printing settings influence the mechanical properties of the printed sample, as can be seen in the extensive review of Popescu *et al.*[27] as well as our Supplementary text and the references therein pointing to studies on the influence of slicing parameters, building orientation and temperature conditions. It is therefore important to keep those parameters constant for consistency purposes between all samples preparation. Starting from the default settings of the 3D printer, we keep the infill density at 100% in order to have a non-porous matrix material. For the building orientation, the samples are printed vertically and each layer is printed with a rotation of 90 degrees from the previous one in order to reduce the anisotropy of the printing that you would obtain when stacking directly the filaments on top of each other. For the temperature conditions, we follow the recommendation of the Ultimaker 3 user manual for PLA[2] for the extruder's temperature at 200ºC and the one of the bed table at 60ºC. For the slicing parameters, the wall/shell thickness of the sample is taken to be equal to the layer height in order to be printed with a single filament in size. Finally, the printing speed is set to 30 mm/s which produces a sample of good quality.

All the compression tests presented in this contribution were performed on the HM3000.3F load frame, manufactured by Humboldt Mfg. Co., with a maximum loading capacity of 50 kN. In order to measure the stress on top of the sample, we use the HM-2300.100 S-Type load cell, which has the same load capacity as the machine and is also manufactured by Humboldt Mfg. Co. The strain is measured directly from the speed of the load plate and it was verified that the deformation of the load cell, which is taken in account with this method, had a negligible effect on the results.

Mechanical model for 3D printed PLA

In this section we propose an elasto-plastic model to fit the stress-strain curves, plotted in Fig. 1, of the PLA cylinders printed as described above. Note that we can appreciate the reproducibility of the experiments as the curves superpose to a precision

[1] http://ultimaker.com/materials
[2] http://ultimaker.com/en/resources/22225-how-to-print-with-ultimaker-pla

level hard to obtain experimentally on natural materials.

We can observe on that figure that the material does not behave in a linear elastic manner at first but rather displays a non-linear phase due to strain measurement errors[28] (e.g. bedding error). Relatively quickly, however, the material follows a linear elastic response once the top stress value reaches a threshold of approximately 5 MPa, as seen on Fig. 1. In order to remove the inconsistent bedding error and have the elastic part of all curves superposed for assessing the reproducibility of the results, we shift the origin of vertical strain of each stress-strain curve so it corresponds to the stress value of 15 MPa, a safe arbitrary value of above which linear elasticity is fully observed.

As can be seen on Fig. 1, the elastic properties are extremely consistent between all samples as the elastic parts of the curves completely superpose. We can then measure a Young's modulus of 1375 MPa on the curves of Fig. 1 since the Young's modulus of the material is directly given by the slope of the elastic part in uniaxial compression. Since Poisson's ratio does not play a role in uniaxial compression, we do not measure it and assume the value reported in the literature of 0.45 for our numerical model, as the material is known to be quite incompressible. As a polymer, PLA naturally remains viscoplastic after the printing process. Since this contribution is not focused on quantifying the rate-dependency of the material, we select an arbitrary loading rate of 0.08mm/min for all experiments in this contribution.

The plastic part of the curves in Fig. 1 is decomposed in three different phases. Past the end of elastic behaviour, the material is hardening, which is due to the viscoplasticity of the polymer, until the peak stress is reached. After the peak stress, the material experiences softening, arguably from the shearband forming. Eventually, the material converges to a limit load. Note that the curves on Fig. 1 do not display a limit load per se as the stress increases again at large strains. This is a post-processing artefact stemming from the fact that the sample is compressed above an amount of strain at which the top surface of the sample starts increasing due to the shearband. As a result, even though the stress might have converged to a steady value, the load is increasing because the surface on which the stress is applied enlarges. Due to the technical difficulty to properly take this change of surface area into account in the post-processing step, the stress plotted is calculated by accounting for the initial top surface area only, which can therefore not capture the eventual hardening at large strains. For this reason we decide to disregard the last part of the curves where the load increases and consider for the value of limit load the minimum value of stress achieved after softening.

Our contribution focuses on the influence of the microstructure of the material yield. For this reason, we do not necessarily need to capture in the model the parts of the stress strain curves that corresponds to the intrinsic behaviour of the material, i.e. the hardening from viscoplasticity and the softening from shearbanding. We focus instead on the two end points of the plastic behaviour: the macroscopic yield which corresponds to the onset of plasticity, and the limit load. Fig. 1 shows the calibration of the plasticity model for the 3D printed PLA with a value of the macroscopic yield measured at 78 MPa and the value of the limit load at 55 MPa.

Note that the model selected here is only suggested for the specific printing settings with the testing procedure detailed above and may not be applicable with other parameters as we have shown – non-exhaustively – that many parameters influence the mechanical properties of the printed PLA.

References

1. Mackenzie, J. K. The elastic constants of a solid containing spherical holes. *Proc. Phys. Soc. Sect. B* **63**, 2–11, DOI: https://dx.doi.org/10.1088/0370-1301/63/1/302 (1950).

2. Hashin, Z. & Shtrikman, S. A variational approach to the theory of the elastic behaviour of multiphase materials. *J. Mech. Phys. Solids* **11**, 127–140, DOI: https://dx.doi.org/10.1016/0022-5096(63)90060-7 (1963).

3. Dunn, D. E., LaFountain, L. J. & Jackson, R. E. Porosity dependence and mechanism of brittle fracture in sandstones. *J. Geophys. Res.* **78**, 2403–2417, DOI: https://dx.doi.org/10.1029/jb078i014p02403 (1973).

4. Hoshino, K. Effect of porosity on the strength of the clastic sedimentary rocks. In *Advances in rock mechanics: Proceedings of the 3rd Congress of International Society of Rock Mechanics, Denver, Colorado, September*, vol. IIA, 511–516 (1974).

5. Gurson, A. L. Continuum theory of ductile rupture by void nucleation and growth: Part i—yield criteria and flow rules for porous ductile media. *J. Eng. Mater. Technol.* **99**, 2–15, DOI: https://dx.doi.org/10.1115/1.3443401 (1977).

6. Green, R. J. A plasticity theory for porous solids. *Int. J. Mech. Sci.* **14**, 215–224, DOI: https://dx.doi.org/10.1016/0020-7403(72)90063-x (1972).

7. Lin, J., Sari, M., Alevizos, S., Veveakis, M. & Poulet, T. A heuristic model inversion for coupled thermo-hydro-mechanical modelling of triaxial experiments. *Comput. Geotech.* **117**, 103278, DOI: https://dx.doi.org/10.1016/j.compgeo.2019.103278 (2020).

8. Parker, S. P. *McGraw-Hill Dictionary of Scientific and Technical Terms* (New York : McGraw-Hill, 2003), sixth edn.

9. Desrues, J. *et al.* Localisation precursors in geomaterials? In *Springer Series in Geomechanics and Geoengineering*, 3–10, DOI: https://dx.doi.org/10.1007/978-3-319-56397-8_1 (Springer International Publishing, 2017).

10. Ross, C. T. F. *Mechanics of Solids* (Woodhead Publishing, 1999).

11. Lesueur, M. *Influence of multiphysics couplings across scales: from digital rock physics to induced fault reactivation*. Ph.D. thesis, UNSW Sydney (2020). School of Minerals and Energy Resources Engineering.

12. Hamiel, Y., Lyakhovsky, V. & Agnon, A. Coupled evolution of damage and porosity in poroelastic media: theory and applications to deformation of porous rocks. *Geophys. J. Int.* **156**, 701–713, DOI: https://dx.doi.org/10.1111/j.1365-246x.2004.02172.x (2004).

13. Springmann, M. & Kuna, M. Identification of material parameters of the gurson–tvergaard–needleman model by combined experimental and numerical techniques. *Comput. Mater. Sci.* **33**, 501–509, DOI: https://dx.doi.org/10.1016/j.commatsci.2005.02.002 (2005).

14. Xie, S. Y. & Shao, J. F. Elastoplastic deformation of a porous rock and water interaction. *Int. J. Plast.* **22**, 2195–2225, DOI: https://dx.doi.org/10.1016/j.ijplas.2006.03.002 (2006).

15. Gologanu, M., Leblond, J.-B., Perrin, G. & Devaux, J. Recent extensions of gurson's model for porous ductile metals. In *Continuum Micromechanics*, 61–130, DOI: https://dx.doi.org/10.1007/978-3-7091-2662-2_2 (Springer Vienna, 1997).

16. Tvergaard, V. Influence of voids on shear band instabilities under plane strain conditions. *Int. J. Fract.* **17**, 389–407, DOI: https://dx.doi.org/10.1007/bf00036191 (1981).

17. Fritzen, F., Forest, S., Böhlke, T., Kondo, D. & Kanit, T. Computational homogenization of elasto-plastic porous metals. *Int. J. Plast.* **29**, 102–119, DOI: https://dx.doi.org/10.1016/j.ijplas.2011.08.005 (2012).

18. Besson, J. Damage of ductile materials deforming under multiple plastic or viscoplastic mechanisms. *Int. J. Plast.* **25**, 2204–2221, DOI: https://dx.doi.org/10.1016/j.ijplas.2009.03.001 (2009).

19. Arns, C. *Structure-property Relationships from Digital Images* (VDM Verlag, 2009).

20. Liu, J. *et al.* Computational upscaling of drucker-prager plasticity from micro-CT images of synthetic porous rock. *Geophys. J. Int.* **212**, 151–163, DOI: https://dx.doi.org/10.1093/gji/ggx409 (2017).

21. Lubliner, J. *Plasticity Theory*. Dover books on engineering (Dover Publications, 2008).

22. Permann, C. J. *et al.* MOOSE: Enabling massively parallel multiphysics simulation. *SoftwareX* **11**, 100430, DOI: https://doi.org/10.1016/j.softx.2020.100430 (2020).

23. Imperial College Consortium On Pore-Scale Modelling. Berea sandstone. *figshare* http://dx.doi.org/10.6084/m9.figshare.1153794 (2014).

24. Lesueur, M., Casadiego, M. C., Veveakis, M. & Poulet, T. Modelling fluid-microstructure interaction on elasto-visco-plastic digital rocks. *Geomech. for Energy Environ.* **12**, 1–13, DOI: https://dx.doi.org/10.1016/j.gete.2017.08.001 (2017).

25. Ishutov, S., Hasiuk, F. J., Harding, C. & Gray, J. N. 3d printing sandstone porosity models. *Interpretation* **3**, SX49–SX61, DOI: https://dx.doi.org/10.1190/int-2014-0266.1 (2015).

26. Dizon, J. R. C., Espera, A. H., Chen, Q. & Advincula, R. C. Mechanical characterization of 3d-printed polymers. *Addit. Manuf.* **20**, 44–67, DOI: https://dx.doi.org/10.1016/j.addma.2017.12.002 (2018).

27. Popescu, D., Zapciu, A., Amza, C., Baciu, F. & Marinescu, R. FDM process parameters influence over the mechanical properties of polymer specimens: A review. *Polym. Test.* **69**, 157–166, DOI: https://dx.doi.org/10.1016/j.polymertesting.2018.05.020 (2018).

28. Jardine, R. J., Symes, M. J. & Burland, J. B. The measurement of soil stiffness in the triaxial apparatus. *Géotechnique* **34**, 323–340, DOI: https://dx.doi.org/10.1680/geot.1984.34.3.323 (1984).

Acknowledgements

This work was supported by resources provided by the Australian Research Council (ARC Discovery Grant Nos. DP170104550, DP170104557, Linkage Project LP170100233) and the Pawsey Supercomputing Centre with funding from the Australian Government and the Government of Western Australia. M.V. acknowledges support by the DE-NE0008746- DoE, United States project.